

# Reconfigurable Intelligent Surface-Assisted Cross-Layer Authentication for Secure and Efficient Vehicular Communications

Mahmoud A. Shawky<sup>1</sup>, Student Member, IEEE, Syed Tariq Shah<sup>2</sup>, Michael S. Mollel<sup>3</sup>, Jalil R. Kazim<sup>4</sup>, Member, IEEE, Muhammad Ali Imran<sup>5</sup>, Fellow Member, IEEE, Qammer H. Abbasi<sup>6</sup>, Shuja Ansari<sup>7</sup>, Senior Member, IEEE, Ahmad Taha<sup>8</sup>, Member, IEEE

**Abstract**—Intelligent transportation systems increasingly depend on wireless communication, facilitating real-time vehicular communication. In this context, message authentication is crucial for establishing secure and reliable communication. However, security solutions must consider the dynamic nature of vehicular communication links, which fluctuate between line-of-sight (LoS) and non-line-of-sight (NLoS). In this paper, we propose a lightweight cross-layer authentication scheme that employs public-key infrastructure-based authentication for initial legitimacy detection while using keyed-based physical-layer re-authentication for message verification. However, the latter’s detection probability ( $P_d$ ) decreases with the reduction of the signal-to-noise ratio (SNR). Therefore, we examine using Reconfigurable Intelligent Surface (RIS) to enhance the SNR value directed toward the designated vehicle and consequently improve the  $P_d$ , especially for NLoS scenarios. We conducted theoretical analysis and practical implementation of the proposed scheme using a 1-bit RIS, consisting of  $64 \times 64$  reflective units. Experimental results show a significant improvement in the  $P_d$ , increasing from 0.82 to 0.96 at SNR =  $-6$  dB for an orthogonal frequency division multiplexing system with 128 subcarriers. We also conducted informal and formal security analyses, using Burrows-Abadi-Needham (BAN)-logic, to prove the scheme’s ability to resist passive and active attacks. Finally, the computation and communication comparisons demonstrate the superior performance of the proposed scheme compared to traditional crypto-based methods.

**Index Terms**—BAN-Logic analysis, Cross-layer authentication, Public key infrastructure, Reconfigurable intelligent surface.

## I. INTRODUCTION

Road traffic accidents cause 1.35 million fatalities annually, resulting in about 3,700 deaths per day, and it is expected to rank fifth among the causes of death by 2030 [1]. To address this issue, the World Health Organization has recognised the importance of developing Intelligent Transportation Systems that enable real-time communication from vehicle-to-vehicle (V2V) and vehicle-to-infrastructure (V2I) [2]. Vehicular ad-hoc networks (VANETs) generally consist of three primary components: a trusted authority (TA), roadside units (RSUs), and wireless communication devices located on vehicles, also known as onboard units (OBUs) [3]. Each vehicle transmits a safety-related message containing information on location, speed, and heading at a transmission rate of 100 – 300 msec [4]. This significantly enhances the performance of many traffic-related applications, including safety, mobility, and autonomy. Moreover, it reduces the carbon footprint and facilitates green transportation. However, the open-access nature of

wireless communication makes it vulnerable to typical attacks, such as impersonation and modification. Hence, message authentication is crucial in preventing such attacks [5].

Generally, there are three common types of authentication in VANETs: Public Key Infrastructure (PKI)-based, Identity (ID)-based, and Group Signature (GS)-based [3]. In PKI-based authentication, each vehicle has a pair of private and public keys [6]. The private key is used to generate digital signatures on messages. For verification, the public key is attached to the transmitted message as a digital certificate signed by the TA. In ID-based authentication, the vehicle’s identifier, such as the vehicle identification number, is used as its public key, which can verify signatures generated by the vehicle’s private key. This approach eliminates the need for a separate public key infrastructure, as the identifier serves as the public key [7]. In GS-based authentication, group members generate the signature ( $\sigma$ ) on behalf of the group using their secret keys, while the recipient verifies  $\sigma$  using the group’s public key [8]. The signature is generated so that it cannot be traced back to the specific member who generated it, offering anonymity and privacy preservation. However, these methods require complex cryptographic operations, leading to high computation and communication costs for transmitting and verifying messages.

To overcome this limitation, physical (PHY)-layer authentication techniques have emerged as a promising solution to reduce the overheads associated with upper-layer cryptographic approaches [9]. These techniques employ the unique features of wireless channels, such as channel amplitude and phase responses [10], and the hardware impairments, such as analogue front-end imperfections and carrier frequency offset [11], to discriminate between terminals. Integrating the PHY-layer into the upper-layer authentication approaches enhances the network’s security and scalability, introducing what is referred to as “cross-layer authentication” [12]. The current state-of-the-art cross-layer authentication in VANETs uses crypto-based methods for initial identity verification, and PHY-layer methods for re-authentication [13]. However, the performance of PHY-layer-based techniques in terms of detection and false alarm probabilities depends on the signal-to-noise ratio (SNR). The higher the SNR, the higher the detection probability, and vice versa. Considering the significant wireless channel variations and the instability of vehicular communication links caused by unpredictable obstructions, the re-authentication performance can be adversely affected, posing a challenge.

Reconfigurable Intelligent Surfaces (RISs) have emerged as a novel class of planar meta-material structures that can manipulate and reflect incident electromagnetic waves through dynamic surface property adjustments [14]. By controlling the electromagnetic waves’ reflection and scattering, RISs can en-

M.A. Shawky, J.R. Kazim {m.shawky.1, j.kazim.1}@research.gla.ac.uk, S.T. Shah, M.S. Mollel, M.A. Imran, Q.H. Abbasi, S. Ansari, and A. Taha {syed tariq.shah, michael.mollel, Muhammad.Imran, Qammer.Abbasi, Shuja.Ansari, Ahmad.Taha}@glasgow.ac.uk are with the James Watt School of Engineering, University of Glasgow, UK.

hance wireless communication systems' SNR values, resulting in improved PHY-layer re-authentication performance.

Following is a summary of this paper's contributions:

- 1) This paper extends our prior work introduced in [26] by developing a pseudo-identity-based PHY-layer re-authentication method, following the initial legitimacy detection using PKI-based authentication. This significantly reduces the communication and computation costs of transmitting and verifying a cryptographic signature for every message transmission while maintaining the security and privacy requirements of VANETs.
- 2) For enhanced performance, we demonstrate how the RIS can help improve the PHY-layer authentication's detection probability for non-line-of-sight V2I communication scenarios. Accordingly, we investigated the scheme's performance for RIS-assisted vehicular communication through theoretical analysis and practical experimentation using 1-bit RIS with  $64 \times 64$  reflective elements.
- 3) We demonstrate that the proposed scheme satisfies VANETs' security and privacy requirements and resists passive and active attacks. Our final analysis compares the scheme's computation and communication costs to traditional crypto-based approaches.

The structure of the remainder of this paper is as follows. Section II reviews relevant prior works. Section III presents the proposed scheme. Section IV analyses the scheme's security and privacy. Section V evaluates the scheme's performance. Finally, in Section VI, we provide concluding remarks.

## II. RELATED WORKS

This section reviews existing work on traditional authentication approaches and cross-layer authentication.

### A. Traditional cryptographic signatures-based authentication

This part reviews current authentication designs that seek to alleviate the significant overheads inherent in traditional authentication methods in VANETs. In Asaar et al. [15], and Liu et al. [16], proxy vehicle-based authentication schemes have been proposed to mitigate the computational overhead on RSUs. These schemes adopt an ID-based approach, leveraging the computational resources availability of proxy vehicles to verify signatures on behalf of RSUs. However, a lack of proxy vehicles in some scenarios is a challenge since all signatures must be verified by RSUs, resulting in increased computation and communication loads. In [17], Jiang et al. propose using region trust authorities to deliver efficient vehicle authentication services while reducing the computational load of TA and RSUs. In [18], Lim et al. propose a GS-based solution that addresses the overheads of the TA by introducing a hierarchical structure of RSUs, comprising leader and member RSUs. The leader RSUs are empowered to generate group keys as a group manager, thereby reducing the overheads on the TA. However, a compromised leader RSU can compromise the security and privacy of group members within the region. In [19], Shao et al. propose a batch verification-based authentication scheme that enables recipients to verify multiple received signatures simultaneously. However, the high computation complexity of

bilinear pairing (BP) operations poses a significant challenge. Moreover, this method is susceptible to failure in the presence of a single invalid signature, which can lead to time-consuming singular verification.

In [20], Cui et al. developed an elliptic curve cryptosystem (ECC)-based content-sharing scheme tailored for fifth-generation (5G)-enabled vehicular networks. The authors' approach enables vehicles with content downloading requests to efficiently filter their nearby vehicles to select competent and suitable proxy vehicles. These selected proxy vehicles are then requested to provide content services. Wang et al. [21], and Li et al. [22] proposed conditional privacy-preserving authentication schemes to reduce authentication overheads and promote privacy. By adopting these schemes, vehicles are not required to store any certificates for authentication, and the TA is also relieved of the need to retrieve the real identity of malicious vehicles from certificates. While the previously mentioned methods aim to achieve a higher authentication rate, many suffer from limited network scalability, highlighting the need for more effective solutions to meet the growing demands of vehicular communication systems.

### B. An overview of cross-layer authentication

Wen et al. [12] patented a cross-layer authentication method that uses PKI-based authentication for handshaking and generates a radio frequency fingerprint for re-authentication. In [23]–[25], PKI-based authentication is integrated with the PHY-layer re-authentication using the feature tracking mechanism. This mechanism depends on the spatial and temporal correlation of the wireless channel responses within the coherence period  $T_c$ . Gope et al. [13] propose an approach for incorporating the integrated circuits (ICs) physically unclonable function (PUF) into a pseudo-ID-based authentication. Based on the IC's physical variation ( $P$ ), the PUF method effectively generates an unpredictable response  $R = P(C)$ , where  $C$  is the input challenge.

However, the scalability of hardware imperfections-based techniques is limited, as the false alarm probabilities increase with the number of terminals. This is due to the slight dissimilarities in the hardware impairments extracted features from different devices. For feature tracking-based techniques, the recipient must extensively observe all the communicating terminals' secret features within  $T_c$ , constituting a significant challenge. In this context, it is crucial to consider some parameters when selecting the PHY-layer re-authentication method. These include channel variations, broadcasting rates, computation availability, and communication ranges. In [26], we presented two re-authentication mechanisms: the PHY-layer signature-based identity authentication mechanism (PHY-SIAM) and the PHY-layer feature-tracking mechanism (PHY-FTM). PHY-SIAM is a keyed-based PHY-layer authentication mechanism where the message content is hashed and encapsulated into two orthogonal frequency-division multiplexing (OFDM) symbols. This forms the PHY-layer signature that can only be equalised at the intended receiver's side. PHY-FTM is a feature-tracking mechanism that utilises the high correlation between the channel estimates

of subsequent OFDM symbols to verify message integrity. However, the previous study presented in [26] focused on the re-authentication performance for subsequent transmissions, assuming that the initial authentication was conducted during the first time slot. This study proposes a comprehensive cross-layer authentication scheme that employs PKI-based authentication for handshaking, followed by PHY-SIAM and PHY-FTM as a two-factor re-authentication process. In addition, we investigate the possibility of using the RIS to enhance the re-authentication performance. To the best of our knowledge, this is the first work that introduces a RIS-assisted cross-layer authentication scheme for VANET applications.

### III. RIS-ASSISTED AUTHENTICATION: THE PROPOSED SCHEME

This section describes the system model, discusses the proposed scheme in detail, and explains how the RIS enhances the scheme's performance at low SNR values.

#### A. System modeling

The system model of the proposed RIS-assisted vehicular communication scheme is depicted in Fig. 1. The considered system model consists of the following entities

- *TA*: The TA is a trusted entity for all network terminals, possessing sufficient computational resources to register and revoke any network terminal. It is also responsible for generating and distributing the system's public parameters. In addition, it is the only terminal capable of revealing vehicles' real identities in case of misbehaving (such as constructing an attack or violating traffic laws).
- *RSU*: The RSU authenticates vehicles within range by verifying their broadcasted messages. It is also assumed to have a reliable communication link with the RIS's smart controller, where it can control the phase shift of the RIS elements. The RSU aims to optimise the RIS's configuration to form a directed beam toward the communicating vehicle in the shadowed areas.
- *Vehicle's OBU*: The OBU is a vehicle-mounted wireless communication device with limited computing capabilities. It can authenticate with nearby RSUs to send and receive real-time traffic conditions. We assume that both RSU and OBU are equipped with a single antenna.
- *RIS*: The RIS comprises  $L$  reconfigurable passive reflectors and is deployed to provide reliable communication links between the RSU and vehicles' OBUs (see Fig. 1). By doing so, the reflected signal towards the designated vehicle/RSU can be deliberately strengthened or impaired. Each RIS has a smart controller that allows the RSU to adjust the phase shift of the RIS reflecting units by choosing between different configuration patterns.

The notations used in this paper are summarised in Table I for ease of understanding.

#### B. The proposed authentication scheme

This section provides a detailed discussion of the proposed scheme. In this work, each terminal has a long-term digital

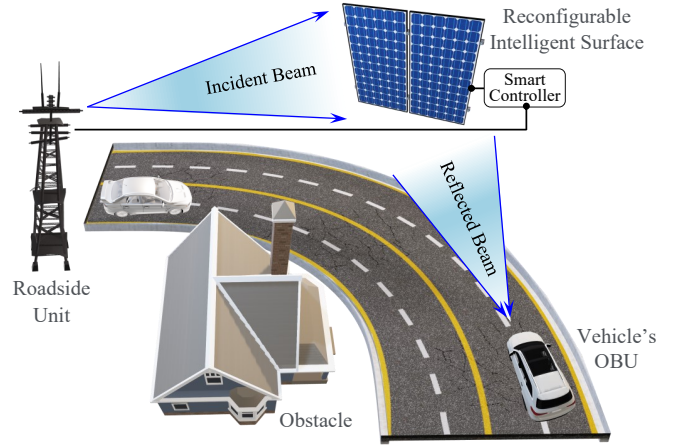


Fig. 1: System modelling

TABLE I: List of notations

Symbol	Definition
$PPs$	The system's public parameters
$\beta, PK_{TA}$	The system's master key and TA's public key
$PK_{V_i}, SK_{V_i}$	$V_i$ 's public and private keys, respectively
$Cert_{V_i}$	$V_i$ 's long-term digital certificate
$T_R$	The certificate validation time
$TID_{V_i}, PID_{V_i}$	$V_i$ 's temporary and pseudo identities
$PK_{R_k}, SK_{R_k}$	$R_k$ 's public and private keys, respectively
$Cert_{R_k}$	$R_k$ 's long-term digital certificate
$TID_{R_k}$	$R_k$ 's temporary identities
$SK_{i-k}$	The shared key between $V_i$ and $R_k$
$\sigma_{V_i}, \sigma_{R_k}$	$V_i$ 's and $R_k$ 's signatures
$\sigma_{V_i}^{PHY}$	$V_i$ 's PHY-layer signature
$\phi_a, \phi_b$	The PHY-layer signature's phase shifts
$T_i, T_r$	signatures' creating and receiving timestamps
$T_\Delta$	Timestamps' expiration period, e.g., [00:00:59]
$P_d, P_{fa}$	The detection and false alarm probabilities

certificate for initial verification and handshaking between two legitimate parties. For re-authentication and secure message verification between vehicles and RSUs, we use PHY-SIAM and PHY-FTM [26] as a two-factor re-authentication method for the OFDM system of  $N$  subcarriers. The proposed scheme comprises four phases, i.e., initialisation, registration, initial authentication, and message signing and verification.

1) *System initialisation phase*: The TA follows the following steps to initialise the system's public parameters.

- The scheme is designed based on the 80-bit security level of the elliptic curve  $E : y^2 = x^3 + ax + b \pmod{p}$ . In this context, we adopted the 160-bit elliptic curve, which is parameterised using the recommended domain settings of "secp160k1" [27], as listed in Table II.
- Based on the generator  $P$ , the TA generates a cyclic group  $\mathbb{G}$  of order  $q$ , which consists of all  $E$ 's points as well as the infinity point  $\mathcal{O}$ .
- The TA chooses the system master key  $\beta \in Z_q^*$ , then computes its related public parameter  $PK_{TA} = \beta.P$ .
- The TA selects two hash functions  $H_1 : \{0, 1\}^* \rightarrow \{0, 1\}^{N_1}$  and  $H_2 : \{0, 1\}^* \rightarrow \{0, 1\}^{2N_2}$  for  $N_2 = 3N/4$ . It also selects the 2-bit Gray code mapping function

TABLE II: The 160-bit  $EC$ 's recommended parameters of "secp160k1" in the Hexadecimal form [27]

Par.	Value
$a$	00000000 00000000 00000000 00000000 00000000
$b$	00000000 00000000 00000000 00000000 00000007
$p$	FFFFFFFF FFFFFFFF FFFFFFFF FFFFFFFF FFFFFFFF FFFFFFFF
$q$	01 00000000 00000000 0001B8FA 16DFAB9A CA16B6B3
$P$	04 3B4C382C E37AA192 A4019E76 3036F4F5 DD4D7EBB 938CF935 318FDCED 6BC28286 531733C3 F03C4FEE

$\mathcal{M}(x_i) \rightarrow \phi_i$  that maps  $x_i$  to  $\phi_i$  as follows.

$$\phi_i = \mathcal{M}(x_i) = \begin{cases} 0 & x_i = [00] \\ \frac{\pi}{2} & x_i = [01] \\ \pi & x_i = [11] \\ \frac{3\pi}{2} & x_i = [10] \end{cases}, \forall i \in [1, N_2] \quad (1)$$

- Finally, the system's public parameters  $PPs$  can be represented by the tuple  $\langle a, b, p, q, P, Pk_{TA}, H_1, H_2, \mathcal{M} \rangle$ .

2) *Registration phase*: The TA registers all terminals before being part of the network by performing the following steps.

- For vehicle registration, the TA checks the vehicle  $V_i$ 's real identity  $RID_{V_i}$ , selects at random  $V_i$ 's secret key  $SK_{V_i} \in Z_q^*$ , and calculates its related public parameter  $PK_{V_i} = SK_{V_i} \cdot P$ . Finally, the TA preloads the tuple  $\langle PPs, SK_{V_i}, Cert_{V_i} \rangle$  onto  $V_i$ 's OBU, where  $V_i$ 's long-term digital certificate  $Cert_{V_i} = \langle PK_{V_i}, T_R, \sigma_{TA} \rangle$ ,  $\sigma_{TA} = \text{Sign}_\beta(PK_{V_i} \| T_R)$  and  $T_R$  is the certificate validation time.
- Each RSU  $R_k$  undergoes the same registration process.
- The TA creates a list of revoked vehicles' and RSUs' digital certificates known as the certificate revocation list  $CRL = \{Cert_1, \dots, Cert_z\}$ , where  $z$  is the total number of revoked vehicles and RSUs. At last, the TA distributes the  $CRL$  among vehicles via RSUs in different regions.

3) *Initial authentication phase*: Consider a scenario where  $V_i$  is within the communication range of  $R_k$  and wants to initiate a secure connection. In this case, both terminals,  $V_i$  and  $R_k$ , exchange certificate-based initial authentication packets for mutual legitimacy detection and extracting a symmetric shared key  $SK_{i-k}$ . The following steps constitute this phase.

- $V_i$  selects at random a temporary identity  $TID_{V_i} \in \{0, 1\}^{N_1}$  and sends  $R_k$  a request to communicate in the form of  $\langle TID_{V_i}, T_1, Cert_{V_i}, \sigma_{V_i} \rangle$ , where the signature  $\sigma_{V_i} = \text{Sign}_{SK_{V_i}}(TID_{V_i} \| T_1 \| Cert_{V_i})$  and  $T_1$  is the attached timestamp.
- Avoiding replay attacks,  $R_k$  checks  $T_1$ 's freshness by testing whether if  $T_r - T_1 \leq T_\Delta$  holds or not. Then,  $R_k$  checks  $V_i$ 's legitimacy by determining if  $Cert_{V_i} \in CRL$  holds or not. After that,  $R_k$  authenticates the received tuple by verifying  $\sigma_{V_i}$  as  $\text{Verify}(\sigma_{V_i})_{PK_{V_i}}$ .
- In response to  $V_i$ 's request,  $R_k$  computes  $SK_{i-k} = PK_{V_i} \cdot SK_{R_k}$  using the Diffie-Hellman key exchanging protocol and sends the tuple  $\langle TID_{R_k}, T_2, Cert_{R_k}, \sigma_{R_k} \rangle$  to  $V_i$ , where  $TID_{R_k}$  is the  $R_k$ 's temporary identity and  $\sigma_{R_k} = \text{Sign}_{SK_{R_k}}(TID_{R_k} \| T_2 \| Cert_{R_k})$ .
- At last,  $V_i$  checks if  $T_r - T_2 \leq T_\Delta$  and  $Cert_{R_k} \in CRL$  hold or not, verifies  $\sigma_{R_k}$  as  $\text{Verify}(\sigma_{R_k})_{PK_{R_k}}$ , and computes its own symmetric key  $SK_{i-k} = SK_{V_i} \cdot PK_{R_k}$ .

- Each  $R_k$  in a coverage area stores a list of communicating vehicles' temporary identities and their associated shared key so that  $list_{R_k} = \{Tuple_1, \dots, Tuple_n\}$ , where  $Tuple_i = \langle Cert_{V_i}, TID_{V_i}, SK_{i-k} \rangle \forall i \in [1, n]$ .

Fig. 2 shows the top-level description flowchart of the initial authentication phase.

4) *Message signing and verification phase*: In this phase, we adopt PHY-SIAM and PHY-FTM proposed in [26] as a two-factor re-authentication process performed at the physical layer. We create a PHY-layer signature used as a lightweight re-authentication technique based on the symmetric shared key  $SK_{i-k}$  and the message payload. Throughout this part,  $\mathbb{C}^{N_x \times N_y}$ ,  $\odot$ ,  $(\cdot)^*$ , and  $[\cdot]^T$  refer to a  $N_x \times N_y$  matrix of complex elements, element-wise multiplication, conjugate, and transpose, respectively. While variables in uppercase and Bold represent matrices. The following steps constitute this phase.

- For each specific number  $Q$  of message ( $m$ ) transmissions,  $V_i$  selects a random  $a_1 \in Z_q^*$  and calculates its related public parameter  $A_1 = a_1 \cdot P$ . Next,  $V_i$  computes its pseudo-identity  $PID_{V_i} = TID_{V_i} \oplus H_1(a_1, PK_{R_k})$ .
- Then,  $V_i$  sends  $R_k$  the message in the form of  $\langle m, PID_{V_i}, A_1, T_3, \sigma_{V_i}^{PHY} \rangle$ , where  $\sigma_{V_i}^{PHY}$  is the PHY-layer signature computed in a 2-step process as follows.

- *Signature preparation step*:  $V_i$  computes two OFDM symbols' phase shifts,  $\Phi_a = [e^{j\phi_{a,1}}, \dots, e^{j\phi_{a,N_2}}]^T \in \mathbb{C}^{N_2 \times 1}$  and  $\Phi_b = [e^{j\phi_{b,1}}, \dots, e^{j\phi_{b,N_2}}]^T \in \mathbb{C}^{N_2 \times 1}$ , where  $\phi_a = \mathcal{M}(H_2(\{SK_{1-2}\}_x \| T_3 \| A_1 \| PID_{V_i} \| m))$ ,  $\phi_b = \mathcal{M}(H_2(\{SK_{i-k}\}_y \| T_3 \| A_1 \| PID_{V_i} \| m))$ , and  $\{.\}_x$  and  $\{.\}_y$  represent the  $x$  and  $y$  coordinates of the elliptic curve point  $SK_{i-k} \in \mathbb{G}$ , respectively.

- *Signature generation step*: In this step,  $V_i$  encapsulates  $\phi_a$  and  $\phi_b$  onto two subsequent OFDM symbols of  $N$  subcarriers and sends it to  $R_k$  at times  $t$  and  $t + \Delta t$  so that the transmitted symbols can be represented as

$$\begin{aligned} \mathbf{S}_1 &= [s_{1,1}, \dots, s_{1,N_2}]^T = \Phi_a \odot \mathbf{X}, \\ \mathbf{S}_2 &= [s_{2,1}, \dots, s_{2,N_2}]^T = \Phi_b \odot \mathbf{X} \end{aligned} \quad (2)$$

where  $\mathbf{X} = [e^{j\psi_1}, \dots, e^{j\psi_{N_2}}]^T \in \mathbb{C}^{N_2 \times 1}$ ,  $\psi_i$  is a uniformly distributed random variable  $\psi_i \sim U[0, 2\pi)$ , and  $\Delta t$  is the transmission time interval. Note that the OFDM symbols in (2) are collectively referred to as  $\sigma_{V_i}^{PHY}$ . Also, we consider the OFDM system as a superposition of  $N$  independently operating narrow-band subsystems.

- $R_k$  receives  $\sigma_{V_i}^{PHY}$  in (2) at times  $t'$  and  $t' + \Delta t$ , which can be represented in the frequency-domain, following the removal of the cyclic-prefix and calculating the Fast Fourier Transform (FFT), as

$$\begin{aligned} \mathbf{R}_1 &= [r_{1,1}, \dots, r_{1,N_2}]^T = (\mathbf{H}_{VR} \odot \mathbf{S}_1) + \mathbf{N}, \\ \mathbf{R}_2 &= [r_{2,1}, \dots, r_{2,N_2}]^T = (\mathbf{H}'_{VR} \odot \mathbf{S}_2) + \mathbf{N}' \end{aligned} \quad (3)$$

where  $\mathbf{H}_{VR} = [|h_{1,1}|e^{j\xi_{1,1}}, \dots, |h_{1,N_2}|e^{j\xi_{1,N_2}}]^T \in \mathbb{C}^{N_2 \times 1}$ ,  $\mathbf{H}'_{VR} = [|h'_{1,1}|e^{j\xi'_{1,1}}, \dots, |h'_{1,N_2}|e^{j\xi'_{1,N_2}}]^T \in \mathbb{C}^{N_2 \times 1}$ ,  $\{|h_{1,i}|, \xi_{1,i}\}$  and  $\{|h'_{1,i}|, \xi'_{1,i}\}$  are the channel amplitude and phase responses of the  $i^{th}$  subcarrier at times  $t'$  and  $t' + \Delta t$ , respectively, and  $\{\mathbf{N}, \mathbf{N}'\}$  are complex additive Gaussian noises  $\mathbb{CN}(0, \sigma_n^2)^{N_2 \times 1}$  with means and

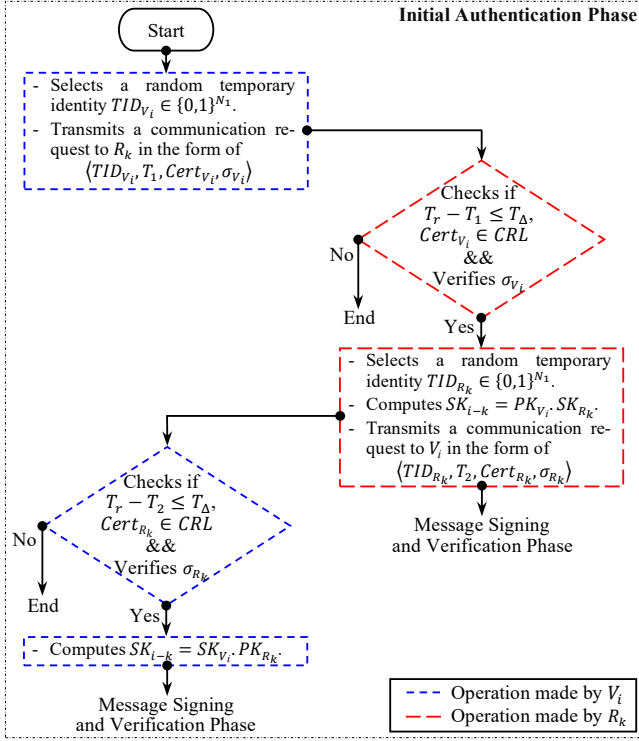


Fig. 2: The top-level description of the initial authentication

variances equal zero and  $\sigma_n^2$ , respectively. Note that  $\mathbf{H}_{VR}$  is highly correlated with  $\mathbf{H}'_{VR}$  for  $\Delta t \leq T_c$ .

- $R_k$  checks  $T_3$ 's freshness, computes  $TID_{V_i} = PID_{V_i} \oplus H_1(A_1.SK_{R_k})$  and finds out if  $TID_{V_i} \in list_{R_k}$  holds or no. If yes,  $R_k$  uses  $SK_{i-k}$  associated with  $TID_{V_i}$  and the message payload  $\langle m, PID_{V_i}, A_1, T_3 \rangle$  to compute  $\phi'_a = \mathcal{M}(H_2(\{SK_{i-k}\}_x \| T_3 \| A_1 \| PID_{V_i} \| m))$  and  $\phi'_b = \mathcal{M}(H_2(\{SK_{i-k}\}_y \| T_3 \| A_1 \| PID_{V_i} \| m))$ .
- Then,  $R_k$  uses a two-factor authentication process, PHY-SIAM and PHY-FTM, in two binary hypothesis testing problems for identity and message verification. This process comprises the following steps.

- *Message verification step using PHY-SIAM:* In this step,  $R_k$  uses the computed  $\phi'_a$  and  $\phi'_b$  to equalise the received PHY-layer signature in (3) by computing  $\mathbf{R}'_1 = \mathbf{R}_1 \odot \Phi'^*_a$  and  $\mathbf{R}'_2 = \mathbf{R}_2 \odot \Phi'^*_b$ , where  $\Phi'_a = [e^{j\phi'_{a,1}}, \dots, e^{j\phi'_{a,N_2}}]^T \in \mathbb{C}^{N_2 \times 1}$  and  $\Phi'_b = [e^{j\phi'_{b,1}}, \dots, e^{j\phi'_{b,N_2}}]^T \in \mathbb{C}^{N_2 \times 1}$ . Since  $\xi_{1,i}$  and  $\xi'_{1,i}$  are highly correlated within  $T_c$ ,  $R_k$  verifies the received message by computing  $\mathbf{C} = [c_1, \dots, c_{N_2}]^T = \mathbf{R}'_1 \odot \mathbf{R}'_2^*$ . Then,  $R_k$  calculates the circular variance  $c.var(\cdot)$  of  $\angle(\mathbf{C}) = [\angle(c_1), \dots, \angle(c_{N_2})]^T$  as

$$v = c.var \left( \sum_{i=1}^{N_2} \arctan \left( \frac{\text{Im}(c_i(t))}{\text{Re}(c_i(t))} \right) \right) \quad (4)$$

where  $c.var$  is defined as

$$\alpha_i = \begin{pmatrix} \cos(\angle(c_i)) \\ \sin(\angle(c_i)) \end{pmatrix}, \bar{\alpha} = \frac{1}{N_2} \sum_{i=1}^{N_2} \alpha_i, \quad (5)$$

$$v = 1 - \|\bar{\alpha}\|$$

where  $\|\cdot\|$  represents the norm function. Avoiding impersonation and modification attacks,  $R_k$  verifies  $\sigma_{V_i}^{PHY}$  in a hypothesis-testing problem given by

$$v \leq \tau_1, \text{ for } \begin{cases} H_0: \Phi'_a = \Phi_a \ \& \ \Phi'_b = \Phi_b \\ H_1: \Phi'_a \neq \Phi_a \ \& \ \Phi'_b \neq \Phi_b \end{cases} \quad (6)$$

where  $\tau_1$  is the threshold value and  $H_0$  and  $H_1$  are the hypotheses that state whether the received message has been successfully authenticated or unauthenticated, respectively. For more information, see reference [26].

- *Message verification step using PHY-FTM:* Based on the OFDM symbols structure of order  $M$  symbols in Fig. 3,  $R_k$  measures the correlation coefficient between the channel observation vector  $\bar{H}_j$  estimated from the reference symbols of the  $j^{\text{th}}$  OFDM symbol and that  $\bar{H}_{j+1}$  of the  $(j+1)^{\text{th}}$  OFDM symbol, starting from  $\sigma_{V_i}^{PHY}$  at  $j = \{1, 2\}$  to the  $M^{\text{th}}$  symbol. Hence, if  $\bar{H}_j$  is highly correlated with  $\bar{H}_{j+1}$ , this means that these symbols are sent from the same transmitter. Otherwise, the received message is discarded. Hence, message verification can be described as a hypothesis-testing process based on the normalised likelihood ratio test (LRT), which is given by

$$\Lambda_{LRT} = \frac{n_{\tau_2} \|\bar{H}_j - \bar{H}_{j-1}\|^2}{\|\bar{H}_{j-1}\|^2} \quad \forall j \in [2, M], \quad (7)$$

$$\Lambda_{LRT} \begin{cases} \leq \tau_2 & H_1 \\ > \tau_2 & H_0 \end{cases}$$

where  $\tau_2 \in [0, 1]$  is the threshold value and  $n_{\tau_2}$  is the normalisation coefficient. The decision rule can be made based on the sequential probability ratio test (SPRT) that sums the LRTs between the  $j^{\text{th}}$  and the  $(j-1)^{\text{th}}$  OFDM symbols  $\forall j \in [2, M]$ . The SPRT-based hypothesis-testing problem can be expressed as

$$\Lambda_j = \frac{n_{\tau_2} \|\bar{H}_{M-j+1} - \bar{H}_{M-j}\|^2}{\|\bar{H}_{M-j}\|^2} \quad \forall j \in [1, M-1], \quad (8)$$

$$\Lambda_{SPRT} = n_{\tau_3} \sum_{j=2}^M \Lambda_j, \Lambda_{SPRT} \begin{cases} \leq \tau_3 & H_1 \\ > \tau_3 & H_0 \end{cases}$$

where  $\tau_3 \in [0, 1]$  is the threshold value and  $n_{\tau_3}$  is the normalisation coefficient. For more information, see reference [26].

- Finally,  $R_k$  accepts or discards the received message from  $V_i$  based on the decision rule of both PHY-SIAM and PHY-FTM hypothesis problems. Accepted messages are those that are identified by both problems as being  $H_0$ . Otherwise, the message will be discarded.

Fig. 4 shows the top-level description flowchart of the message authentication and integrity verification phase.

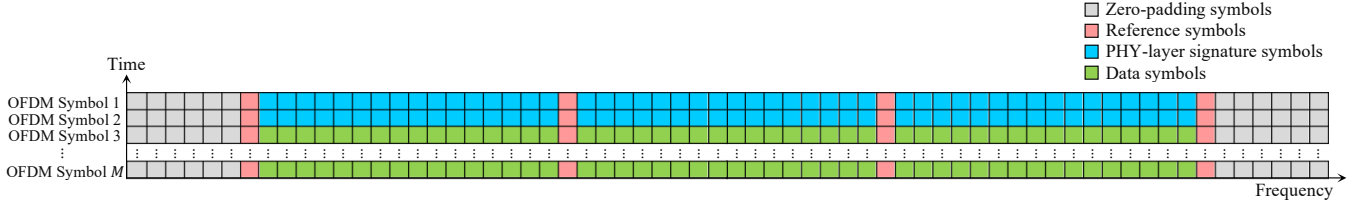


Fig. 3: OFDM symbols' structure for 64 subcarriers

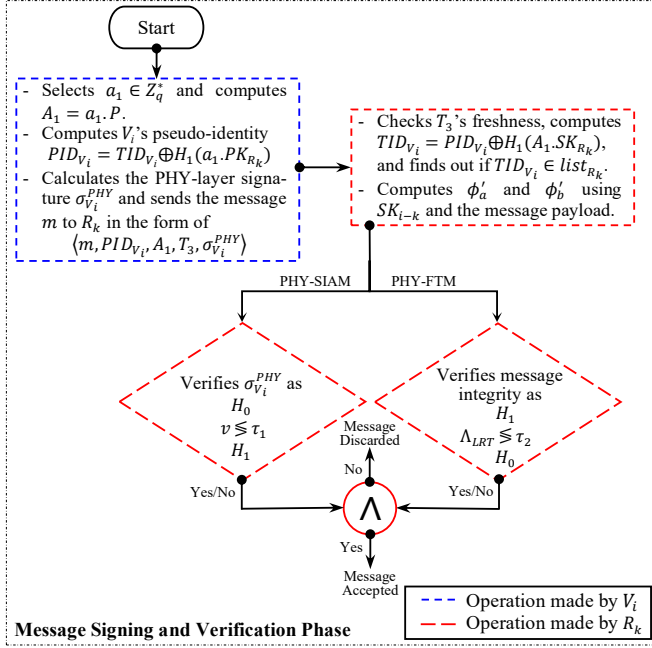


Fig. 4: The top-level description of the message authentication and integrity verification phase

### C. RIS-assisted PHY-layer authentication

One of the challenging issues of PHY-layer authentication is that the detection probability  $P_d$  primarily depends on the received signal's SNR value, whereas  $P_d$  defines the probability of authenticating legitimate users as authorised terminals. A higher SNR value indicates a higher  $P_d$  for an acceptable false alarm probability  $P_{fa}$ , and vice versa, where  $P_{fa}$  defines the probability of authenticating legitimate users as unauthorised terminals. This makes the PHY-layer authentication impractical in long-range and non-line-of-sight (NLoS) vehicular communications. In this challenging scenario, RIS can enhance the power of the received signal at the receiver for the NLoS communication, see Fig. 1. As a result, the proposed scheme can effectively authenticate the received messages from the vehicles in the shadowing areas. Thus, the received signals in (3) for the  $i^{th}$  subcarrier is the superposition of  $L$  multipath components coming from  $L$  RIS's reflective elements and can be reformulated as

$$\begin{aligned} r_{1,i} &= (\mathbf{H}_{VI} \odot \mathbf{H}_{IR}) \boldsymbol{\omega}_\theta s_{1,i} + n_i, \\ r_{2,i} &= (\mathbf{H}'_{VI} \odot \mathbf{H}'_{IR}) \boldsymbol{\omega}_\theta s_{2,i} + n'_i \end{aligned} \quad \forall i \in [1, N_2] \quad (9)$$

where  $\mathbf{H}_{VI} = [|h_{2,1}|e^{j\xi_{2,1}}, \dots, |h_{2,L}|e^{j\xi_{2,L}}] \in \mathbb{C}^{1 \times L}$ ,  $\mathbf{H}_{IR} = [|h_{3,1}|e^{j\xi_{3,1}}, \dots, |h_{3,L}|e^{j\xi_{3,L}}] \in \mathbb{C}^{1 \times L}$ , and  $\boldsymbol{\omega}_\theta = [e^{j\omega_1\theta_1}, \dots, e^{j\omega_L\theta_L}]^T \in \mathbb{C}^{L \times 1}$ .  $\mathbf{H}_{VI}$  and  $\mathbf{H}_{IR}$  represents the channel responses from  $V_i$  to RIS and from RIS to  $R_k$ , respec-

tively. While  $\boldsymbol{\omega}_\theta$  defines the phase shift matrix related to the  $L$  reflective elements of the RIS, where  $\theta_l$  and  $\omega_l$  defines the  $l^{th}$  reflective element phase shift value and state, respectively  $\forall l \in [1, L]$ , for example,  $\theta_l = \pi$  and  $\omega_l \in \{0, 1\}$  for a 1-bit RIS. Note that  $\{\mathbf{H}_{VI}, \mathbf{H}_{IR}\}$  is highly correlated with  $\{\mathbf{H}'_{VI}, \mathbf{H}'_{IR}\}$  within  $T_c$ . The RSU in each region optimises the RIS configuration  $\boldsymbol{\omega}_\theta$  to maximise the power of the received signals at the side of the intended user. Hence, improving the receiver operating characteristics (ROCs;  $P_d$  versus  $P_{fa}$ ) of the two-factor re-authentication process at poor SNRs.

## IV. SECURITY AND PRIVACY ANALYSES

This section investigates how the proposed scheme satisfies the security and privacy requirements of VANETs.

### A. Security and privacy informal analysis

1) *Message authentication*: The proposed scheme offers legitimacy detection and ensures message integrity for the following reasons:

- For legitimacy detection, the recipient  $V_i/R_k$  verifies the sender's legitimacy  $R_k/V_i$  by checking if  $Cert_{V_i/R_k} \in CRL$ , where  $\sigma_{TA} \in Cert_{V_i/R_k}$  is signed using  $\beta \in \mathbb{Z}_q^*$  and verified by the recipient using  $PK_{TA} \in PPs$ , which is infeasible to be forged under the difficulty of solving the elliptic curve discrete logarithm problem (ECDLP). In addition, the transmitted tuple  $\langle TID_{V_i/R_k}, T_1, Cert_{V_i/R_k}, \sigma_{V_i/R_k} \rangle$  is verified for its integrity using the signature  $\sigma_{V_i/R_k}$  that is signed using  $V_i/R_k$ 's secret key  $SK_{V_i/R_k}$  and verified by the recipient using  $PK_{V_i/R_k} \in Cert_{V_i/R_k}$ .
- For message authentication at subsequent transmission slots, the tuple  $\langle m, PID_{V_i}, A_1, T_3, \sigma_{V_i}^{PHY} \rangle$  is verified by  $R_k$  for its integrity in a two-factor authentication process, PHY-SIAM and PHY-FTM, that's infeasible to be forged for the following reasons: A) The phase shifts,  $\Phi_a$  and  $\Phi_b$ , in (2) are computed based on the shared key  $SK_{i-k} \in \mathbb{G}$  and masked by  $\mathbf{X} = \{e^{j\psi_1}, \dots, e^{j\psi_{N_2}}\}$ , where  $\psi_i$  is a uniformly distributed random variable  $\sim U[0, 2\pi)$ , which makes it infeasible for an adversary to differentiate between  $\Phi_a$  and  $\Phi_b$  and  $\mathbf{X}$ . B) The high correlation coefficient between subsequent channel observation vectors  $\{\bar{H}_{j-1}, \bar{H}_j\}$  in (7)  $\forall j \in [2, M]$  or  $\{\bar{H}_j, \bar{H}_{j+1}\}$  in (8)  $\forall j \in [1, M-1]$  helps in detecting modification attempts in the message payload.

2) *Privacy preservation*: In the proposed scheme, vehicles communicate using their temporary identities  $TID_{V_i}$  at the first transmission slot, while pseudo identities  $PID_{V_i}$  are used at subsequent transmissions. This preserves users' real

identities  $RID_{V_i}$  from exposure as no network terminals possess  $RID_{V_i}$  or even the link between  $RID_{V_i}$  and its associated long-term digital certificates  $Cert_{V_i}$  except for the TA. Only the TA is authorised to expose  $RID_{V_i}$  in cases of misbehaviour (for example, when the vehicle constructs an attack or when a driver drives an unregistered vehicle).

3) *Unlinkability*: For each  $Q$  number of message transmissions per session,  $V_i$  uses a different pseudo-identity  $PID_{V_i} = TID_{V_i} \oplus H_1(a_1.PK_{R_k})$ , where  $a_1 \in Z_q^*$  is dynamically updated for each session. Hence, no parameter is used twice per session, thereby avoiding location-tracking attacks.

4) *Traceability and revocation*: Each RSU in a specific area can report misbehaving vehicles to the TA by sending its associated digital certificate  $Cert_{V_i}$ . The TA, in turn, reveals its associated real identity, appends  $Cert_{V_i}$  to the *CRL*, and distributes the updated *CRL* among vehicles via RSUs.

5) *Resistance to passive and active attacks*: This part discusses the scheme's resistance against typical adversarial attacks. By considering an adversary, Eve acts as a passive attacker and listens to the communicating terminals' broadcasted messages to deduce any useful information about the symmetric key  $Sk_{i-k}$ . In this scenario, Eve attempts to deduce the shared key either during the initial authentication phase (case 1) or during the message signing and verification phase (case 2). In case 1,  $Sk_{i-k}$  is calculated using the Diffie-Hellman key exchanging protocol. This makes it difficult for Eve to compute  $Sk_{i-k}$  due to the difficulty of solving the ECDLP. In case 2, Eve has difficulty deducing the value of  $Sk_{i-k}$  from the PHY-layer signature  $\sigma_{V_i}^{PHY}$  due to the following: 1) The signature generation step is dependent on the dynamically updated parameters  $\langle T_i, A_i, PID_{V_i}, m \rangle$ , which results in different outputs,  $\Phi_a$  and  $\Phi_b$ , under the same shared key  $Sk_{i-k}$ . In addition, The received  $\sigma_{V_i}^{PHY}$  in (3) is dependent on the spatially and temporally varying channel phase responses  $\xi_i$  and  $\xi'_i$  that masks  $\phi_{a,i}$  and  $\phi_{b,i}$ , respectively. 2) For  $y = H_2(x)$ , it is difficult for Eve to determine the input variable  $x$  from the hashed variable  $y : \{0, 1\}^{N_2}$ . In this scenario, we consider Eve to be an active attacker who is capable of constructing the following types of attacks:

- *Modification resistance*: In this attack, Eve tries to modify the message payload either during the initial authentication phase (case 1) or during the message signing and verification phase (case 2). In case 1, the recipient  $R_k/V_i$  verifies the received tuple  $\langle TID_{V_i/R_k}, T_i, Cert_{V_i/R_k}, \sigma_{V_i/R_k} \rangle$  for its integrity based on the attached signature  $\sigma_{V_i/R_k}$ . For this attack to be successful, Eve must modify the message contents and forge a valid signature, which is computationally intractable due to the difficulty of solving the ECDLP. In case 2, Eve must modify the message contents  $\langle m, PID_{V_i}, A_i, T_i \rangle$  and forge a valid signature  $\sigma_{V_i}^{PHY}$ . Without any knowledge of the shared key  $Sk_{i-k}$ , Eve is unable to correctly estimate the values of  $\Phi_a$  and  $\Phi_b$  needed to generate a valid signature. Accordingly, this type of attack can be easily detected.
- *Impersonation resistance*: In this attack, Eve tries to impersonate the communicating vehicle  $V_i$  during the initial authentication phase. For this attack to be successful, Eve

must generate a valid signature  $\sigma_{V_i}$  using the  $V_i$ 's secret key  $Sk_{V_i}$ , which cannot be forged due to the difficulty of solving the ECDLP. Accordingly, it is hard to compute a valid shared key  $Sk_{i-k}$  used for generating  $\sigma_{V_i}^{PHY}$  during the message signing and verification phase. Hence, the proposed scheme is resistant to this type of attack.

- *Replay resistance*: In this attack, Eve repeats the transmission of a previously captured message either during the initial authentication phase (case 1) or during the message signing and verification phase (case 2). In both cases, each transmission is accompanied by a fresh timestamp  $T_i$  that helps the recipient detect this type of attack by testing whether  $T_r - T_i \leq T_\Delta$  holds. Hence, the proposed scheme is resistant to replay attacks.

## B. Security proof using BAN-logic formal analysis

The Burrows-Abadi-Needham (BAN) security proof is a formal methodology that offers a rigorous approach to evaluate the security of authentication protocols. The BAN approach is grounded in a formal model of authentication protocols and employs inference rules to analyse the knowledge and beliefs of principals involved in the protocol. Due to its effectiveness, the BAN methodology has been extensively adopted for analysing and verifying the security of authentication protocols in diverse settings such as computer networks, web communications, smart cards, and mobile devices. This study employs the BAN logic analysis to scrutinise the security of the proposed method against various types of attacks, such as replay, man-in-the-middle, and impersonation attacks.

1) *Notations*: In BAN-logic, security properties are expressed and argued using the following symbols.

- $A \equiv X$ :  $A$  believes that the proposition of  $X$  is true.
- $A \triangleleft X$ :  $A$  sees  $X$  denotes that principal  $A$  has received a message that includes the value  $X$ .
- $A \mid \sim X$ :  $X$  has been transmitted to  $A$  at some point, and  $A$  has subsequently believed the proposition  $X$ .
- $A \mid \implies X$ :  $A$  has control over the value  $X$  and has the authority or jurisdiction to manipulate or modify it.
- $A \xleftrightarrow{k} B$ :  $A$  and  $B$  share a secret key  $k$ , which they use to securely communicate with each other.
- $A \xrightarrow{k} B$ :  $k$  denotes the public key attributed to  $A$ .
- $\{X\}_k$ : The shared key  $k$  is used to encrypt  $X$ .
- $\#(X)$ : It represents a fresh message  $X$ .

2) *Rules*: A set of deductive rules are used to analyse initial beliefs and protocol messages exchanged between participants and make inferences about the security properties of the protocol. These rules are listed and defined in Table III.

3) *Goals*: The primary objective of BAN-logic is to demonstrate the validity of the proposed scheme by accomplishing the following set of goals.

- *Goal 1*:  $R_k \mid \equiv (R_k \xleftrightarrow{Sk_{i-k}} V_i)$ .
- *Goal 2*:  $R_k \mid \equiv (V_i \mid \equiv M_1)$ .
- *Goal 3*:  $V_i \mid \equiv (V_i \xrightarrow{Sk_{i-k}} R_k)$ .
- *Goal 4*:  $V_i \mid \equiv (R_k \mid \equiv M_2)$ .
- *Goal 5*:  $R_k \mid \equiv (M_3)$ .

TABLE III: The rules involved in the BAN-logic analysis

No.	Rule	BAN-logic representation	Definition
$R_1$	Message rule for a shared key	$\frac{A \equiv(A \xrightarrow{K} B), A \triangleleft \{X\}_K}{A \equiv(B \sim X)}$	If $A$ believes in $K$ and $A$ received $X$ encrypted by $K$ , then $A$ believes $B$ said $X$
$R_2$	Message rule for a public key	$\frac{A \equiv(B \xrightarrow{K} A), A \triangleleft \{X\}_{k-1}}{A \equiv(B \sim X)}$	If $A$ believes $K$ is $B$ 's public key and receives $X$ encrypted with $B$ 's private key, then $A$ believes $B$ said $X$
$R_3$	Nonce verification rule (NVR)	$\frac{A \equiv\#(X), A \equiv(B \sim X)}{A \equiv(B \equiv X)}$	If $A$ believes $X$ is fresh and that $B$ said $X$ , then $A$ believes $B$ believes $X$
$R_4$	Jurisdiction rule (JR)	$\frac{A \equiv(B \Rightarrow X), A \equiv(B \equiv X)}{A \equiv X}$	If $A$ believes $B$ has jurisdiction over $X$ and that $B$ believes $X$ , then $A$ believes $X$
$R_5$	Freshness rule (FR)	$\frac{A \equiv\#(X)}{A \equiv\#(X, Y)}$	Freshness of one part ensures the freshness of the entire formula

4) *Idealised forms*: The following points formulate the idealised messages for the proposed method.

- $M_1$ :  $V_i \rightarrow R_k$ :  $\{TID_{V_i}, T_1, Cert_{V_i}\}_{SK_{V_i}}$ , where  $Cert_{V_i} = \{PK_{V_i}, T_R\}_\beta$ .
- $M_2$ :  $R_k \rightarrow V_i$ :  $\{TID_{R_k}, T_2, Cert_{R_k}\}_{SK_{R_k}}$ , where  $Cert_{R_k} = \{PK_{R_k}, T_R\}_\beta$ .
- $M_3$ :  $V_i \rightarrow R_k$ :  $\{m, PID_{V_i}, A_1, T_3, \sigma_{V_i}^{PHY}\}$ , where  $\sigma_{V_i}^{PHY} = \{m, PID_{V_i}, A_1, T_3\}_{SK_{i-k}}$ .

5) *Assumptions*: The fundamental assumptions underlying the BAN-logic security proof are as follows.

- $A_1$ :  $R_k | \equiv \#(T_1)$ .
- $A_2$ :  $V_i | \equiv \#(T_2)$ .
- $A_3$ :  $R_k | \equiv \#(T_3)$ .
- $A_4$ :  $R_k | \equiv (TA \xrightarrow{K_{TA}} R_k)$ .
- $A_5$ :  $V_i | \equiv (TA \xrightarrow{K_{TA}} V_i)$ .
- $A_6$ :  $\frac{R_k | \equiv (TA \xrightarrow{PK_{TA}} R_k), R_k \triangleleft \{PK_{V_i}, T_R\}_\beta}{R_k | \equiv (V_i \xrightarrow{PK_{V_i}} R_k)}$ .
- $A_7$ :  $\frac{V_i | \equiv (TA \xrightarrow{PK_{TA}} V_i), V_i \triangleleft \{PK_{R_k}, T_R\}_\beta}{V_i | \equiv (R_k \xrightarrow{PK_{R_k}} V_i)}$ .
- $A_8$ :  $R_k | \equiv (V_i \Rightarrow M_3)$ .

6) *Implementation*: The security proof of the proposed protocol is presented as follows.

- *Step 1*: Upon receipt of message  $M_1$  from  $V_i$ ,  $R_k$  applies  $A_4$  and  $Cert_{V_i} \in M_1$  to  $A_6$ , resulting in the following outcome:  $O_1$ :  $R_k | \equiv (V_i \xrightarrow{PK_{V_i}} R_k)$ . Accordingly,  $R_k$  computes  $SK_{i-k} = PK_{V_i} \cdot SK_{R_k}$  and have  $O_2$ :  $R_k | \equiv (R_k \xrightarrow{SK_{i-k}} V_i)$ , achieving *Goal 1*.
- *Step 2*: By applying  $O_1$  and  $M_1$  to  $R_2$  from Table III, the outcome is  $O_3$ :  $R_k | \equiv (V_i | \sim M_1)$ . Next, by applying  $A_1$  and  $M_2$  to  $R_5$  from Table III, we have  $O_4$ :  $R_k | \equiv \#(M_1)$ . Accordingly, by applying  $O_4$  and  $O_3$  to  $R_3$  from Table III, we have  $R_k | \equiv (V_i | \equiv M_1)$ , achieving *Goal 2*.
- *Step 3*: Upon receipt of message  $M_2$  from  $R_k$ ,  $V_i$  applies  $A_5$  and  $Cert_{R_k} \in M_2$  to  $A_7$ , resulting in the following outcome:  $O_5$ :  $V_i | \equiv (R_k \xrightarrow{PK_{R_k}} V_i)$ . Accordingly,  $V_i$  computes  $SK_{i-k} = SK_{V_i} \cdot PK_{R_k}$  and have  $O_6$ :  $V_i | \equiv (V_i \xrightarrow{SK_{i-k}} R_k)$ , achieving *Goal 3*.
- *Step 4*: By applying  $O_5$  and  $M_2$  to  $R_2$  from Table III, the outcome is  $O_7$ :  $V_i | \equiv (R_k | \sim M_2)$ . Next, by applying  $A_2$  and  $M_2$  to  $R_5$  from Table III, we have  $O_8$ :  $V_i | \equiv \#(M_2)$ . Accordingly, by applying  $O_8$  and  $O_7$  to  $R_3$  from Table III, we have  $V_i | \equiv (R_k | \equiv M_2)$ , achieving *Goal 4*.
- *Step 5*: Upon receipt of message  $M_3$  from  $V_i$ ,  $R_k$  applies  $O_2$  and  $\sigma_{V_i}^{PHY} \in M_3$  to  $R_1$  from Table III, then we have

$O_9$ :  $R_k | \equiv (V_i | \sim M_3)$ . Next, by applying  $A_3$  and  $M_3$  to  $R_5$  from Table III, we have  $O_{10}$ :  $R_k | \equiv \#(M_3)$ . Then, by applying  $O_{10}$  and  $O_9$  to  $R_3$  from Table III, we have  $O_{11}$ :  $R_k | \equiv (V_i | \equiv M_3)$ . Finally, by applying  $A_8$  and  $O_{11}$  to  $R_4$  from Table III, we have  $O_{12}$ :  $R_k | \equiv (M_3)$ , achieving *Goal 5*.

## V. PERFORMANCE EVALUATION

This section analyses the theoretical and practical aspects of RIS-assisted PHY-layer authentication performance, followed by detailed computation and communication comparisons.

### A. Theoretical analysis of the PHY-layer authentication

In order to evaluate the ROCs of the proposed method, it is crucial to evaluate the probability density function (PDF) for the phase estimate ( $\Theta$ ) of  $\mathbf{C} = \mathbf{R}'_1 \odot \mathbf{R}'_2^*$ , where  $\mathbf{R}'_1$  and  $\mathbf{R}'_2$  denote the equalised received PHY-layer signature, given by the element-wise multiplication of  $\mathbf{R}_1$  in (3) and  $\Phi_a^*$ , and  $\mathbf{R}_2$  in (3) and  $\Phi_b^*$ , respectively. In the case of  $\{\Phi_a, \Phi_b\}$  at the transmitting side  $V_i$  are equivalent to  $\{\Phi'_a, \Phi'_b\}$  at the receiving side  $R_k$ , the phase distribution of  $\mathbf{C}$  for varying SNR values can be formulated according to [26] as follows.

$$P(\Theta | \Gamma) = \frac{1}{2\pi} e^{-\Gamma} + \frac{1}{\sqrt{\pi}} (\sqrt{\Gamma} \cos \Theta) \cdot e^{-\Gamma \sin^2 \Theta} [1 - \mathbb{Q}(\sqrt{2\Gamma} \cos \Theta)] \quad (10)$$

where

$$\Gamma = \frac{|h_i|^2 \cdot E_S^2}{\sigma_n^2}, \quad (11)$$

$$\mathbb{Q}(x) = \frac{1}{\sqrt{2\pi}} \int_x^\infty e^{-t^2/2} dt$$

where  $E_S$  is the symbol energy. Fig. 5 presents  $P(\Theta | \Gamma)$  for different SNR values (i.e.,  $\Gamma \in [0, 25]$  dB). As indicated in (4), the circular variance of  $\angle(\mathbf{C})$  with a specific order of  $N_2$  is denoted as  $v$ , and this quantity satisfies the central limit theorem (CLT). Therefore,  $v$ 's distribution  $\mathcal{F}(x)$  follows a normal distribution with a mean ( $\mu_{H_0}$ ) equal to the variance of  $P(\Theta)$  for a given  $\Gamma$  value and a variance equal to  $\sigma_{H_0}^2$ . Thus, the following formulation can express  $v$ 's cumulative distribution function (CDF) for both hypotheses.

$$\phi(x | \mu_{H_i}, \sigma_{H_i}^2) = \frac{1}{2} \left[ 1 + \operatorname{erf} \left( \frac{x - \mu_{H_i}}{\sqrt{2\sigma_{H_i}^2}} \right) \right], \forall i \in \{0, 1\} \quad (12)$$

In this context, we define  $P_d = \phi(x | \mu_{H_0}, \sigma_{H_0}^2) \Big|_{x=\tau_1}$



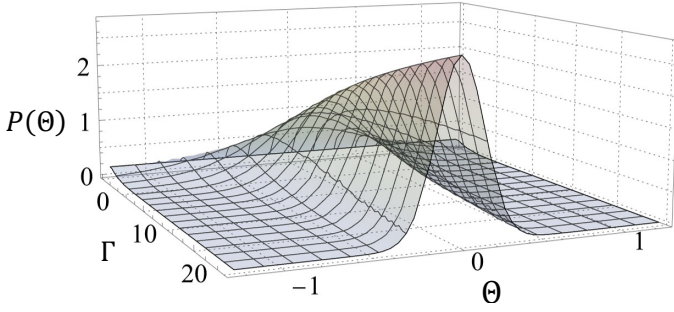


Fig. 5:  $P(\Theta | \Gamma)$  in (10) at different given  $\Gamma \in [0, 25]$  dB

and  $P_{fa} = \phi(x | \mu_{H_1}, \sigma_{H_1}^2) \Big|_{x=\tau_1}$  for a threshold value  $\tau_1$  of the hypothesis testing problem in (6). As illustrated in (11), the channel fading coefficient, represented by  $|h_i|$ , is a critical factor in determining the value of  $\Gamma$  while maintaining a constant value of  $E_s$  and noise variance  $\sigma_n^2$ . Generally, the received signal at the recipient side comprises various multipath components originating from distinct scatterers. Nonetheless, in this study, our focus is solely on the RIS path connecting the communicating terminals, as the impact of the remaining scatterers is consistent regardless of whether the RIS being switched ON or OFF. The channel components of the  $i^{th}$  subcarrier in both scenarios, considering the RIS turned ON and OFF, have been expressed in (3) and (9), respectively. Accordingly, the presence of the RIS can improve the SNR towards the communicating vehicle by configuring the reflective elements in a way that constructively interferes in a specific direction. This can be achieved by controlling the RIS electromagnetic behaviour by optimising  $\omega_\theta$  in (9) to maximise the  $\Gamma$  value in (11). By doing so, the system's performance at a certain SNR value, denoted as  $\Gamma = X$  dB, without the RIS can be equal to its performance at a lower SNR value,  $\Gamma = X - \Delta X$  dB, with the RIS. A higher  $\Gamma$  value signifies a decrease in the overlapping between the distributions of both hypotheses,  $\mathcal{F}(x)|_{H_0}$  and  $\mathcal{F}(x)|_{H_1}$ , due to a lower value of  $\mu_{H_0}$  for  $\mathcal{F}(x)|_{H_0}$  relative to  $\mu_{H_1}$  for  $\mathcal{F}(x)|_{H_1}$ . This improvement enhances the detection performance while maintaining an acceptable false alarm probability ( $a_1$ ). Hence, the optimisation of the system's threshold value ( $\tau_1$  in (6)) can be computed by utilising the following formula [26].

$$\tau_1 = \arg \max_{\tau_1'} \text{erf} \left( \frac{\tau_1' - \mu_{H_1}}{\sqrt{2\sigma_{H_1}^2}} \right) \leq 2a_1 - 1 \quad (13)$$

### B. Practical experimentation of the RIS-assisted method

In order to demonstrate the practicality of the proposed RIS-assisted PHY-layer authentication method, we conducted a hardware implementation using a 1-bit RIS consisting of 4096 reflective elements arranged in a two-dimensional  $64 \times 64$  grid, along with a universal serial radio peripheral (USRP) equipped with two channels (denoted as  $Ch_0$  and  $Ch_1$ ) that functioned as the transmitter ( $T_x$ ) and receiver ( $R_x$ ), representing  $R_k$  and  $V_i$ , respectively. The antennas used for  $T_x$  and  $R_x$  are of the two-horn type, with the  $T_x$  antenna beam adjusted perpendicular to the RIS reflecting surface and located 3 meters away from the centre. On the other hand, the  $R_x$

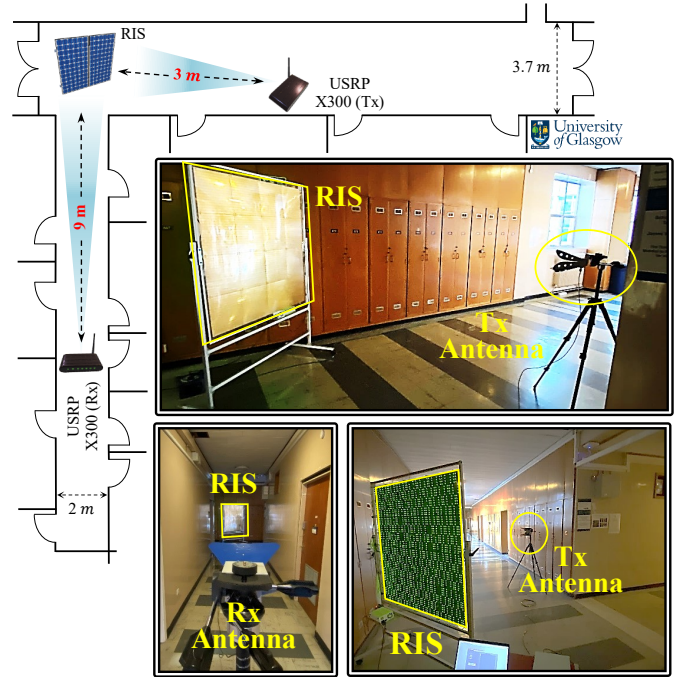


Fig. 6: Experiment setup of the RIS-assisted method

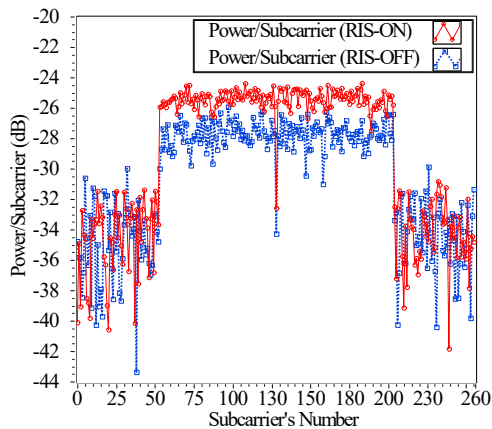
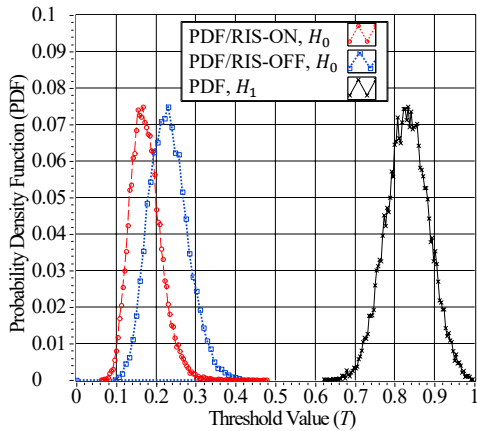
antenna was situated 9 meters away from the RIS, with an NLoS path between it and the  $T_x$  antenna, and its beam set at a 45-degree angle from the line connecting the  $T_x$  antenna to the RIS. Different views of the experimental setup are presented in Fig. 6 while Table IV shows the experimental settings.

We set the carrier frequency  $F_c$  to 3.75 GHz for 5G-V2I communication, the  $T_x$  and  $R_x$  gains to 20 dB and 5 dB, respectively, and the sampling rates for both channels to 200 KHz. We implemented a range of OFDM systems with varying numbers of subcarriers including 64, 128, and 256, and cyclic prefix (CP) lengths of 16, 32, and 64. To determine the optimal configuration associated with the location of the receiving antenna, we utilised the Hadamard codebook. The Hadamard codebook comprises a number of Hadamard matrices that provide a set of binary and orthogonal phase shift states ( $\omega_l, \forall l \in [1, L]$ ) that can be used to modify the reflection of incoming electromagnetic waves in a desired direction or with a preferred phase shift by applying these values to the reflective elements. Accordingly, we implemented the proposed re-authentication method by transmitting two consecutive OFDM symbols with the same structure presented in Fig. 3, representing the PHY-layer signature  $\sigma_{V_i}^{PHY}$ .

Fig. 7 shows the received OFDM symbol in the frequency domain following the removal of the CP and applying the FFT. This figure presents the received power in dB for each subcarrier when the RIS is ON and OFF. It can be seen that the power of the subcarriers carrying data has increased by approximately 2 dB with the activation of the RIS. This improvement is significant, especially for NLoS scenarios. Fig. 8 shows the PDF for hypothesis  $H_0$  when the RIS is ON and OFF and for hypothesis  $H_1$  for  $N = 64$  subcarriers and SNR = 5 dB. The figure demonstrates that the activation of the RIS results in a reduction of the mean value for  $\text{PDF}|_{H_0}$  compared to when the RIS is off. This reduction leads to a decrease in

TABLE IV: Experimental settings

Par.	Value	Description
$F_c$	3.75 GHz	Carrier frequency
$T_x$ (Gain)	20 dB	The transmitter gain
$R_x$ (Gain)	5 dB	The receiver gain
$N$	64, 128, 256	Number of subcarriers
CP length	16, 32, 64	The cyclic prefix length
SR	200 KHz	The sampling rate for the $T_x$ and $R_x$
Antennas types	Horn	$T_x$ and $R_x$ antennas types
$T_x \leftrightarrow$ RIS	3 meters	The distance between the $T_x$ and RIS
RIS $\leftrightarrow$ $R_x$	9 meters	The distance between the RIS and $R_x$

Fig. 7: The received symbol's power for each subcarrier at  $N = 256$  subcarriersFig. 8: Distributions of both hypotheses  $H_{0,1}$  with and without the RIS for  $N = 64$  subcarriers and SNR = 5 dB

the overlap between  $\text{PDF}|_{H_0}$  and  $\text{PDF}|_{H_1}$ , providing superior ROC curves under low SNR conditions.

Fig. 9 illustrates the ROC curve for varying SNR values  $\text{SNR} \in \{0, -3, -6\}$  dB,  $N = 64$  subcarriers, and with and without the use of the RIS. The figure demonstrates that decreasing the SNR value reduces  $P_d$  for a given  $P_{fa}$ . This result arises from the increasing overlap between both hypotheses as the SNR decreases. Furthermore, the figure indicates that activating the RIS leads to improved ROC curves. For example, when the RIS is off, the  $P_d$  is approximately 0.92, as shown in Fig. 9(b). However, with the RIS enabled, the  $P_d$  increases to approximately 0.99 for  $P_{fa} \sim 0.2$ , thereby demonstrating the ability of the RIS to enhance the authentication performance.

Additionally, we evaluate the ROC for different numbers of subcarriers  $N = \{64, 128, 256\}$  and fixed SNR value of  $-6$  dB, as presented in Fig. 10. Since  $v$  in (4) represents the circular variance of a specific number of  $N_2 = \frac{3N}{4}$  values, it follows the CLT. Hence, increasing the number of subcarriers results in an increase in  $N_2$ , which reduces the variance of  $\mathcal{F}(x)|_{H_0}$  and minimises the overlap with  $\mathcal{F}(x)|_{H_1}$ , thereby improving the authentication performance. The enhanced ROC curves obtained in Fig. 10 affirm the effectiveness of increasing the number of subcarriers. Moreover, activating the RIS leads to an increase in the  $P_d$  for a given  $P_{fa}$ . As shown in Fig. 10(b), when the RIS is off, the  $P_d$  is roughly 0.82. However, with the RIS enabled, the  $P_d$  increases to approximately 0.96 for  $P_{fa} \sim 0.2$ , thus demonstrating the beneficial impact of the RIS in enhancing authentication performance.

### C. Comparison of computation and communication costs

This subsection presents the computation and communication analyses of the proposed method and shows that it outperforms traditional approaches.

1) *Comparison of computation cost:* This part provides a detailed analysis of the computation comparison. Table VI provides a summary of the running time for various crypto-based operations measured in [28] using the MIRACL cryptographic library [29] and a device equipped with an Intel Core I7 – 6700 processor. In Table VI, the notations  $\{T_{sm}^{BP}, T_{pa}^{BP}\}$  and  $\{T_{sm}^{ECC}, T_{pa}^{ECC}\}$  denote the computational time for the BP-based and ECC-based scale multiplication and point addition, respectively. Furthermore, we evaluated the computational time for the mapping operation  $T_M$ , and the circular variance operation in (5) denoted as  $T_{c.var}$ . The latter was insignificant compared to the values presented in Table VI. Consequently, we have incorporated these results to accurately quantify the total computation cost of the proposed method and ensure a fair comparison.

In our proposed scheme, the EC signature generation process incurs a cost of approximately  $1T_{sm}^{ECC}$ , while the verification process costs  $2T_{sm}^{ECC}$ . Based on this, the computation cost of transmitting  $n$  messages from a single vehicle using our method can be expressed as  $[2T_{sm}^{ECC} + \lceil \frac{n}{Q} \rceil (2T_{sm}^{ECC} + T_h) + n(T_h + T_M)]$ . The first term accounts for the signature generation and the secret key agreement, the second term accounts for the dynamically updating pseudo-identity after every  $Q$  transmitted messages, and the third term accounts for generating  $\sigma_{V_i}^{PHY}$ . On the other hand, the verification time can be expressed as  $[2T_{sm}^{ECC} + \lceil \frac{n}{Q} \rceil (T_{sm}^{ECC} + T_h) + n(T_h + T_M + T_{c.var})]$ . The first term corresponds to the initial signature verification, and the second and third terms verify the pseudo-identity for every  $Q$  transmitted message and  $\sigma_{V_i}^{PHY}$ , respectively. Thus, the total computation cost can be expressed as  $(0.6436 + 0.3228\lceil \frac{n}{q} \rceil + 0.001n) msec$ .

In Cui et al. [20], the computation cost for verifying  $n$  received messages is  $[(n+2)T_{sm}^{ECC} + (n-1)T_{pa}^{ECC} + (2n)T_h] = (0.6412 + 0.3262n) msec$ , while for Wang et al. [21] and Li et al. [22], this value is  $[(3n+2)T_{sm}^{BP} + (2n)T_{pa}^{BP} + (n)T_h] = (1.388 + 2.0866n) msec$  and  $[(3n+2)T_{sm}^{BP} + (3n)T_{pa}^{BP} + (n)T_h] = (1.388 + 2.0884n) msec$ , respectively.

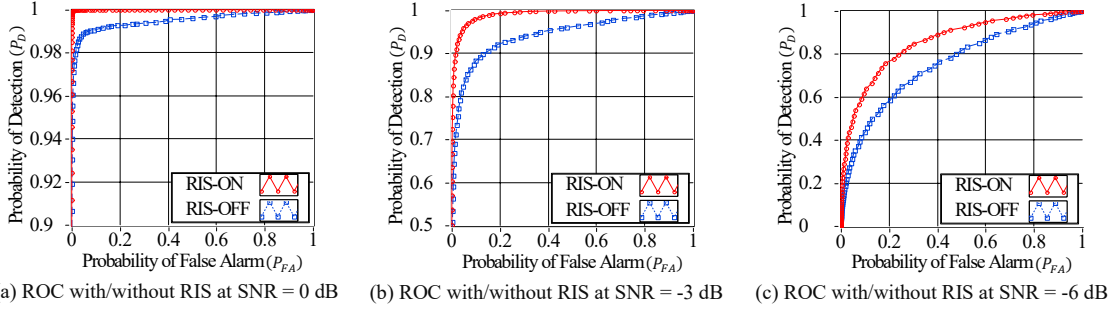


Fig. 9: The ROCs with and without the RIS at different SNRs and  $N = 64$  subcarriers

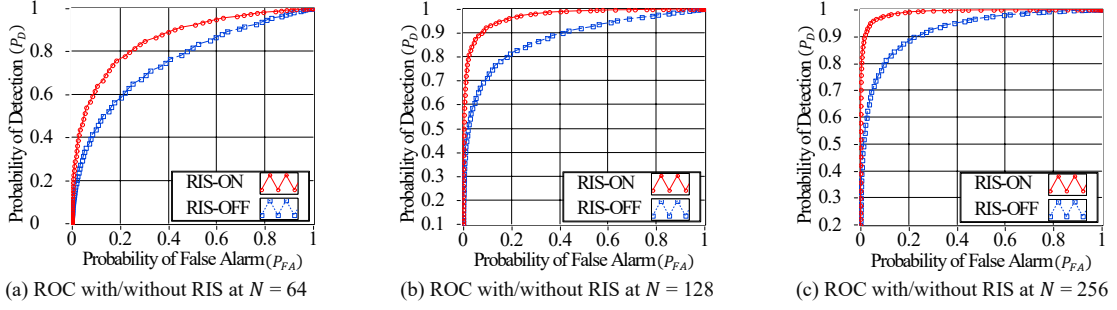


Fig. 10: The ROCs with and without the RIS at different numbers of subcarriers and  $\text{SNR} = -6$  dB

TABLE V: Computation and communication comparisons

Schemes	Computation cost (msec)		Communication cost (bytes)
	Signature generation	Signature verification of $n$ messages	
Cui et al. [20]	$3T_{sm}^{ECC} + 3T_h$	$(n+2)T_{sm}^{ECC} + (n-1)T_{pa}^{ECC} + (2n)T_h$	$124n$
Wang et al. [21]	$2T_{sm}^{BP} + 2T_{pa}^{BP} + T_h$	$(3n+2)T_{sm}^{BP} + (2n)T_{pa}^{BP} + (n)T_h$	$300n$
Li et al. [22]	$3T_{sm}^{BP} + 2T_{pa}^{BP} + T_h$	$(3n+2)T_{sm}^{BP} + (3n)T_{pa}^{BP} + (n)T_h$	$408n$
Our scheme	$2T_{sm}^{ECC} + \lceil \frac{n}{Q} \rceil (2T_{sm}^{ECC} + T_h) + n(T_h + T_M)$	$2T_{sm}^{ECC} + \lceil \frac{n}{Q} \rceil (T_{sm}^{ECC} + T_h) + n(T_h + T_M + T_{c.var})$	$148 + 112n$

TABLE VI: The time required for various crypto operations

Symbol	The operation definition	Run time
$T_{sm}^{BP}$	BP-based scale multiplication in $\mathbb{G}_1$	0.6940
$T_{pa}^{BP}$	BP-based point addition in $\mathbb{G}_1$	0.0018
$T_{sm}^{ECC}$	ECC-based scale multiplication in $\mathbb{G}$	0.3218
$T_{pa}^{ECC}$	ECC-based point addition in $\mathbb{G}$	0.0024
$T_h$	One way hashing operation	0.0010

To illustrate the comparison, Fig. 11 displays the computation cost required to verify 1000 received messages from a single user. Our proposed scheme exhibits the lowest computation cost compared to its best competitors.

2) *Comparison of communication cost* : This part provides a detailed comparison of communication costs. For the 80-bit security level of the proposed scheme, the elliptic curve group is denoted as  $\mathbb{G}$ , where  $|\mathbb{G}| = 40$  bytes and  $Z_q^* = 20$  bytes. For the same security level, the bilinear pairing is denoted as  $\bar{E} : \mathbb{G}_1 \times \mathbb{G}_1 \rightarrow \mathbb{G}_T$ , where  $\bar{P}$  is the generator of the elliptic curve  $\bar{E} : y^2 = x^3 + x \text{ mod } \bar{p}$ , with  $|\mathbb{G}_1| = 128$  bytes and  $Z_q^* = 20$  bytes. Moreover, the size of hashed values using the SHA-1 hashing operation is 20 bytes, and the timestamp has a size of 4 bytes.

In the proposed scheme, the communication cost of transmitting  $n$  messages is determined by the size of

the tuple  $\langle TID_{V_i}, T_1, (PK_{V_i}, T_R, \sigma_{TA}), \sigma_{V_i} \rangle$  during the first transmission slot, as well as the size of the tuple  $\langle PID_{V_i}, A_1, T_3, \sigma_{V_i}^{PHY} \rangle$  for  $n$  subsequent transmissions. Specifically,  $\{PK_{V_i}, A_1\} \in \mathbb{G}$ , and the length of  $TID_{V_i}$  and  $PID_{V_i}$  is 20 bytes each. The sizes of  $\sigma_{TA}$  and  $\sigma_{V_i}$  are 40 bytes each, while the lengths of  $T_R$ ,  $T_1$ , and  $T_3$  are 4 bytes each. The size of  $\sigma_{V_i}^{PHY}$  is 48 bytes. Therefore, the total communication cost for transmitting  $n$  messages is  $[(20 + 2 \times 4 + 3 \times 40) + (20 + 40 + 4 + 48)n] = (148 + 112n)$  bytes. In Cui et al. [20], the signature is represented by the tuple  $\langle PID_j^1, PID_j^2, \delta_j, D_j, T_j \rangle$ , where  $\{PID_j^1, D_j\} \in \mathbb{G}$ ,  $\{PID_j^2, \delta_j\} \in Z_q^*$ , and  $T_j$  denotes the timestamp. Thus, the total size of the signature is  $(2 \times 40 + 2 \times 20 + 4) = 124$  bytes. In Wang et al. [21], the signature is represented by the tuple  $\langle R_{u_i}, T'_{u_i}, \varrho_{u_i}, PK_{TA}, t_i \rangle$ , where  $\{R_{u_i}, T'_{u_i}\} \in \mathbb{G}_1$ ,  $\{\varrho_{u_i}, PK_{TA}\} \in Z_q^*$ , and  $t_i$  represents the timestamp. Thus, the total size of the signature is  $(2 \times 128 + 2 \times 20 + 4) = 300$  bytes. Similarly, Li et al. [22] represent a signature as  $\langle R_{u_i}, K'_{u_i}, KG'_{u_i}, \varrho_{u_i}, t_i \rangle$ , where  $\{R_{u_i}, K'_{u_i}, KG'_{u_i}\} \in \mathbb{G}_1$ ,  $\varrho_{u_i} \in Z_q^*$ , and  $t_i$  denotes the timestamp. The total size of this signature is  $(3 \times 128 + 20 + 4) = 408$  bytes. Fig. 12 shows the communication cost required for transmitting 1000 messages received from a single user. The figure reveals that the proposed scheme exhibits the lowest communication cost compared to its best rivals.

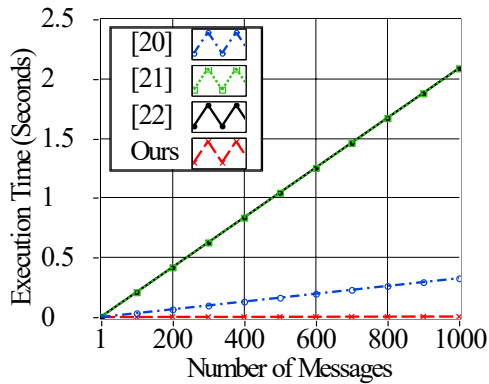


Fig. 11: The computation cost of verifying 1000 messages at  $Q = 100$

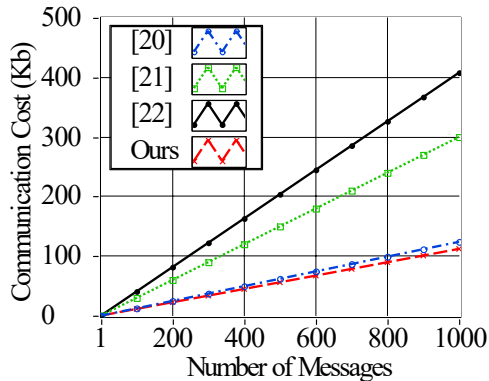


Fig. 12: The communication cost of sending 1000 messages

## VI. CONCLUSIONS

This paper proposes an authentication scheme that utilises the RIS to enhance the detection probability of the PHY-layer authentication in NLoS conditions while still adhering to the security and privacy requirements of VANETs. The theoretical and experimental results demonstrate the effectiveness of the RIS in improving authentication performance. We have performed informal and formal (BAN-logic) analyses to verify the scheme's security resistance against typical attacks. Additionally, we have conducted a computation and communication comparison to demonstrate that the proposed method reduces overheads, resulting in a computation cost savings of over 98% compared to existing methods in [20]–[22], and communication cost savings of approximately 10%, 62%, and 72% compared to [20], [21], and [22], respectively. Our future work will explore the possibility of incorporating the PHY-layer secret key extraction as an alternative key agreement technique and implementing it in outdoor scenarios.

## REFERENCES

- [1] World Health Organization, "Road Traffic Injuries", 2021, available at: <https://www.who.int/news-room/fact-sheets/detail/road-traffic-injuries>
- [2] World Health Organization (WHO), "Intelligent Transport Systems (ITS) for in-Vehicle and Infrastructure Safety: an Evidence-based Analysis", Geneva, Switzerland, 2016.
- [3] M. A. Al-Shareeda, M. Anbar, I. Hasbullah, and S. Manickam, "Survey of Authentication and Privacy Schemes in Vehicular ad hoc Networks", *IEEE Sensors Journal*, vol. 21, no. 2, pp. 2422-2433, Jan. 15.
- [4] S. Grafling, P. Mahonen, and J. Riihijarvi, "Performance Evaluation of IEEE 1609 WAVE and IEEE 802.11p for Vehicular Communications", *ICUFN Conference*, pp. 344-348, 2010.
- [5] F. Qu, Z. Wu, F. -Y. Wang and W. Cho, "A Security and Privacy Review of VANETs", *IEEE Trans. on Intelligent Transportation Systems*, vol. 16, no. 6, pp. 2985-2996, Dec. 2015.
- [6] M. Raya, and J. P. Hubaux, "The security of vehicular ad hoc networks", in *Proc. 3<sup>rd</sup> ACM Workshop Security Ad Hoc Sensor Networks*, pp. 11–21, Nov. 2005.
- [7] A. Shamir, "Identity-based cryptosystems and signature schemes", in *Proc. Workshop Theory Applications Crypto. Technology*, vol. 196, pp. 47–53, 1984.
- [8] D. Chaum, and E. V. Heyst, "Group Signatures", *Workshop on the Theory and Application of Crypto. Tech.*, vol. 547, pp. 257-265, 1991.
- [9] L. Xiao, L. J. Greenstein, N. B. Mandayam, and W. Trappe, "Using the Physical Layer for Wireless Authentication in Time-Variant Channels", *IEEE Trans. on Wireless Communications*, vol. 7, no. 7, Jul. 2008.
- [10] J. Liu, and X. Wang, "Physical Layer Authentication Enhancement Using Two-Dimensional Channel Quantization", *IEEE Trans. on Wireless Communications*, vol. 15, no. 6, Jun. 2016.
- [11] H. Fang, X. Wang, and L. Hanzo, "Learning-Aided Physical Layer Authentication as an Intelligent Process", *IEEE Trans. on Communications*, vol. 67, Nov. 2018.
- [12] H. Wen, J. Zhang, R. Liao, J. Tang, and F. Pan, "Cross-Layer Authentication Method based on Radio Frequency Fingerprint", US 10251058 B2, United States Patent, Apr. 2019.
- [13] P. Gope, A. K. Das, N. Kumar, and Y. Cheng, "Lightweight and Physically Secure Anonymous Mutual Authentication Protocol for Real-Time Data Access in Industrial Wireless Sensor Networks", *IEEE Trans. on Industrial Informatics*, vol. 15, no. 9, Sep. 2019.
- [14] J. Rains et al., "High-Resolution Programmable Scattering for Wireless Coverage Enhancement: An Indoor Field Trial Campaign", *IEEE Trans. on Antennas and Propagation*, vol. 71, no. 1, pp. 518-530, Jan. 2023.
- [15] M. R. Asaar et al., "A Secure and Efficient Authentication Technique for Vehicular Ad-Hoc Networks", *IEEE Trans. on Vehicular Technology*, vol. 67, no. 6, pp. 5409-5423, Jun. 2018.
- [16] Y. Liu, L. Wang and H. -H. Chen, "Message Authentication Using Proxy Vehicles in Vehicular Ad Hoc Networks", *IEEE Trans. on Vehicular Technology*, vol. 64, no. 8, pp. 3697-3710, Aug. 2015.
- [17] Y. Jiang, S. Ge, and X. Shen, "AAAS: An Anonymous Authentication Scheme Based on Group Signature in VANETs", *IEEE Access*, vol. 8, pp. 98986-98998, 2020.
- [18] K. Lim, W. Liu, X. Wang, and J. Joung, "SSKM: Scalable and Secure Key Management Scheme for Group Signature Based Authentication and CRL in VANET", *Electronics*, vol. 8, no. 11, 2019.
- [19] J. Shao, X. Lin, R. Lu, and C. Zuo, "A Threshold Anonymous Authentication Protocol for VANETs", *IEEE Trans. on Vehicular Technology*, vol. 65, no. 3, pp. 1711-1720, Mar. 2016.
- [20] J. Cui, J. Chen, H. Zhong et al., "Reliable and Efficient Content Sharing for 5G-Enabled Vehicular Networks", *IEEE Trans. on Intelligent Transportation Systems*, vol. 23, no. 2, pp. 1247-1259, Feb. 2022.
- [21] Y. Wang, Y. Liu, and Y. Tian, "ISC-CPPA: Improved-Security Certificateless Conditional Privacy-Preserving Authentication Scheme With Revocation", *IEEE Trans. on Vehicular Technology*, vol. 71, no. 11, pp. 12304-12314, Nov. 2022.
- [22] J. Li, Y. Ji et al., "CL-CPPA: Certificate-less conditional privacy-preserving authentication protocol for the internet of vehicles", *IEEE Internet of Things Journal*, vol. 6, no. 6, pp. 10332–10343, Dec. 2019.
- [23] J. Wang, Y. Shao, Y. Ge, and R. Yu, "Physical-Layer Authentication based on Adaptive Kalman Filter for V2X Communication", *Vehicular Communications*, vol. 26, Jul. 2020.
- [24] S. Althunibat, V. Sucasas, G. Mantas, and J. Rodriguez, "Physical-Layer Entity Authentication Scheme for Mobile MIMO Systems", *IET Communications*, vol. 12, pp. 712-718, Mar. 2018.
- [25] H. Wen, and P.-H. Ho, "Physical Layer Technique to Assist Authentication Based on PKI for Vehicular Communication Networks", *KSII Trans. on Internet and Info. Sys.*, vol. 5, no. 2, Feb. 2011.
- [26] M. A. Shawky, M. Usman, M. A. Imran et al., "Adaptive Chaotic Map-based Key Extraction for Efficient Cross-Layer Authentication in VANETs", *Vehicular Communications*, vol. 39, Feb. 2023.
- [27] Certicom Research, *Standards for Efficient Cryptography, SEC 2: Recommended Elliptic Curve Domain Parameters 1.0*, pp. 9–10, Sep. 2000.
- [28] J. Cui, X. Zhang, H. Zhong, Z. Ying, and L. Liu, "RSMA: Reputation System-Based Lightweight Message Authentication Framework and Protocol for 5G-Enabled Vehicular Networks", *IEEE Internet of Things Journal*, vol. 6, no. 4, pp. 6417-6428, Aug. 2019.
- [29] Shamus Software Ltd., Miracl library. Available: <http://www.shamus.ie/index.php?page=home>